Advances in Nano Research, *Vol. 10, No. 3 (2021) 211-219*
DOI: https://doi.org/10.12989/anr.2021.10.3.211

Analyzing corrosion rates of TiO_2 nanotubes/titanium separation passive layer under surface and crystallization changes

I. Zamudio Torres*[1,2], A. Sosa Domínguez[3a], J.J. Pérez Bueno[1b], Y. Meas[1c], M.L. Mendoza López[4d] and A. Dector[5e]

[1]*Centro de Investigación y Desarrollo Tecnológico en Electroquímica, S.C., Parque Tecnológico Sanfandila, Pedro Escobedo, Querétaro, México*
[2]*Universidad Juárez Autónoma de Tabasco, Avenida Universidad S/N, Zona de La Cultura, Col. Magisterial, Centro, Villahermosa, Tabasco, 86040, México*
[3]*Universidad Autónoma de Querétaro, Facultad de Química, Cerro de las Campanas s/n C.P. 76010, Cto. Universitario, Centro Universitario, Santiago de Querétaro, Querétaro, México*
[4]*Tecnológico Nacional de México, Instituto Tecnológico de Querétaro, Av. Tecnológico s/n Esq. M. Escobedo, Col. Centro, Santiago de Querétaro, Querétaro, México*
[5]*CONACYT, Universidad Tecnológica de San Juan del Río, Av. La Palma No. 125, Vista Hermosa, San Juan del Río, Querétaro, México*

(*Received May 13, 2020, Revised October 19, 2020, Accepted October 21, 2020*)

Abstract. The evaluation of the corrosion resistance of titanium with a TiO_2 nanotubes top layer was carried out (TiO_2 NT). These nanostructures were evolved into anatase nanoparticles without heat treatment in an aqueous medium, which is a novel phenomenon. This work analyzes the layer between the nanotube bottom and the substrate, which is thin and still susceptible to corrosion. The bottom of TiO_2 nanotubes having Fluor resulting from the synthesis process changed between amorphous to crystalline anatase with a crystallite size of about 4 nm, which influenced the corrosion rates. Four kinds of samples were evaluated. A) NT by Ti anodizing; B) NTSB for Ti plates, either modifying its surface or anodizing the modified surface; C) NT-480 for anodized Ti and heat-treated (480°C) for reaching the anatase phase; D) NTSB-480 for Ti plates, first, modifying its surface using sandblast, after that, anodizing the modified surface, and finally, heat-treated to 480°C to compare with samples having induced crystallization and passivation. Four electrochemical techniques were used to evaluate the corrosion rates. The surfaces having TiO_2 nanotubes with a sandblast pre-treatment had the highest resistance to corrosion.

Keywords: nano-tubes; photocatalytic material; characterization and application; nano-materials; nanostructured crystals

1. Introduction

The polarization resistance technique has been widely used to monitor the corrosion rate (Sumi *et al*. 2017, Supraja *et al*. 2017). The parameter R_p, which is the polarization resistance, is obtained from the $i_{corr} = B/R_p$ equation and B is derived from the Tafel portion of the polarization curves, which necessarily implies the application of the polarization curve technique (Al-Mobarak *et al*. 2011). In the same way, to perform the determination of the corrosion rate, the Tafel extrapolation method of a potentiodynamic polarization curve is used (Bolat *et al*. 2015, Bosch and Bogaerts 1996, Bosch *et al*. 2001, Chang *et al*. 2011, Dhibar *et al*. 2013). However, this method requires that the anodic and cathodic portion have a Tafelian behavior (Fouda and Wahed 2011).

Electrochemical Impedance Spectroscopy (EIS) has been established as a tool of importance to investigate mechanisms of electrochemical reactions, measure dielectric properties, and to explore the corrosion resistance of materials (Kuş and Mansfeld 2006). This technique describes the electrical resistance using an alternating current circuit, which is equivalent to $E = IZ$, where Z represents the impedance of the circuit, unlike the resistance, the impedance of an AC circuit depends on the frequency of the signal that is applied (McIntyre and Mercer 2010).

The Electrochemical Frequency Modulation (EFM) technique resembles the LPR and EIS techniques so that a non-destructive, double frequency wave disturbance with an amplitude of ± 10 mV to ± 20 mV around the E_{corr}, is applied simultaneously to the material and the alternating current density responses are measured at higher frequencies than the input frequencies (Mazare *et al*. 2016). The EFM technique is fast and validates its results with the values of causality. Electrochemical impedance spectroscopy and electrochemical frequency modulation have a significant advantage since they are non-destructive techniques to study corrosion (Jayaraman *et al*. 2010, Mazare *et al*. 2016, Sumi *et al*. 2017).

*Corresponding author, Ph.D., Professor,
E-mail: zit408@msn.com
[a] Professor, E-mail: adrian.sosa@uaq.mx
[b] Professor, E-mail: jperez@cideteq.mx
[c] Professor, E-mail: yunnymeas@cideteq.mx
[d] Professor, E-mail: mluisaml@yahoo.com
[e] Professor, E-mail: andres_dector@live.com

Copyright © 2021 Techno-Press, Ltd.

ISSN: 2287-237X (Print), 2287-2388 (Online)

Nowadays, the nanotubes of titania obtained by anodizing titanium have been of growing interest to study the photocatalysis in water (Xu *et al*. 2021, Zamudio Torres *et al*. 2016a, b). TiO_2 nanotubes used as templates increment their applications and they are currently investigated in the electrochemical process of the oxygen reduction reaction ORR (Jovanović *et al*. 2020, Noh *et al*. 2020), oxygen evolution reaction OER (Genova-Koleva *et al*. 2019, Schlicht *et al*. 2019), hydrogen evolution reaction HER (Liu *et al*. 2020, Tho *et al*. 2020), and water splitting or water electrolysis (Ge *et al*. 2017). Lithium-ion batteries (Wang *et al*. 2017) or sodium-ion batteries (Li *et al*. 2021, Zhao *et al*. 2017) studies include designs of anodes using TiO_2 nanotubes. They have been proved in UV photo-detectors (Ouyang *et al*. 2018). The reduction of CO_2 is another use for these semiconductor structures (Gu *et al*. 2021). Additionally, the reduction of Cr (VI) has been investigated (Wang *et al*. 2021). Titanium is used in implants, but also TiO_2 nanotubes biocompatibility has been investigated (Chen 2021).

Nanotubes are synthesized mainly by electrochemical anodic oxidation but also using the template technique, the solvothermal method, or the hydrothermal method (Ge *et al*. 2017, Zhou *et al*. 2017).

In recent years, the color variates of TiO_2 nanotubes increased their absorption favoring their photo/electro-catalysis applications (Xu *et al*. 2021, Zhou *et al*. 2017).

Below the TiO_2 nanotubes layer, there is a passive layer that does not completely protect the metallic titanium substrate. This work analyzes the layer between the nanotube bottom and the substrate, which is thin and still susceptible to the substrate active corrosion, which was evidenced by the corrosion rates associated with it, measured using four different electrochemical techniques. This is a further in-depth study of our previously published works (Zamudio Torres *et al*. 2016a, b), which showed a novel phenomenon of amorphous TiO_2 nanotubes transformation into anatase nanoparticles attributed to reactions of the content of Fluor resulting from the synthesis process. So, the bottom of TiO_2 nanotubes changed from amorphous to crystalline anatase having a crystallite size of about 4 nm, which influenced the corrosion rates.

Furthermore, the effect of the different Ti and Ti treatments with TiO_2 nanotubes (Santamaria *et al*. 2017, Sierra-Uribe *et al*. 2017, Shang *et al*. 2018, Fraoucene *et al*. 2019) on the corrosion behavior was investigated by polarization curves, polarization resistance, EIS and modulation of electrochemical frequency in a 5% by weight NaCl solution.

2. Materials and methods

Ti samples were of industrial use. Two kinds of Ti surfaces were anodized: 1) using sandblasting at 100 psi pressure, Al_2O_3 particles with 3 mm in size were used as abrasive, this lets increasing the mechanical properties of the TiO_2 nanotubes layer, avoiding detachment, and 2) a weak-polished titanium. After each treatment, the samples were cleaned by sonication for 5 min.

Table 1 List identifying the treatment applied to each sample. The symbols — and • specify without or with treatment, respectively

Sample	Anodizing	Sand-blast	Annealing (480°C)	Surface composition	SEM
Ti	—	—	—	Ti	
NT	•	—	—	NH_4TiOF_3	Fig. 1(a)
NT-480	•	—	•	TiO_2 anatase	Fig. 1(b)
NTSB	•	•	—	NH_4TiOF_3	Fig. 1(c)
NTSB-480	•	•	•	TiO_2 anatase	Fig. 1(d)

were cleaned by sonication for 5 min.

The anodizing solution had NH_4F 0.095 M, as a source of fluoride ions. The solution consisted of a mixture of ethylene glycol 98% v/v and water 2% v/v dispersing the F^-. For the electrochemical anodizing of the Ti plates, a DC power supply was used.

In order to obtain the anatase phase in the nanotubes, heat treatment on two samples was applied (see Table 1). The samples were introduced in a furnace at room temperature, then a ramp of 10°C/min was employed until it reached 480°C; this temperature was maintained for one h.

The anodizing consisted of two phases: first, a ramp of 6 V each minute, until reaching 60 V; second, constant voltage anodizing (60 V) was carried out for 2 h. The configuration used was of two electrodes, with titanium plates as anode and cathode. The experiments were conducted at room temperature.

The samples were analyzed by Scanning Electron Microscopy (SEM, JEOL model JSM 7800F at 10 kV of acceleration voltage with secondary electron detector).

Measurements were performed using a Gamry Instrument Potentiostat/Galvanostat/ZRA. This includes a Gamry framework system based on the ESA400, Gamry applications with DC105 for DC corrosion measurements, EIS300 for Electrochemical Impedance Spectroscopy, and EFM 140 for Electrochemical Frequency Modulation measurements. Echem Analyst 6.25 software was used for plotting, graphing, and fitting data. In all the different corrosion tests used in this research, NaCl at 5% w/v was used, 1 cm^2 was the geometric area exposed.

Polarization curves were registered between ± 150 mV, using a scan rate of 2 mV/s, prior to measurements, the specimens were maintained in the solution for 5 min. The potential applied around the voltage in the reference Saturate Calomel Electrode (SCE) was about ± 20 mV. EIS studies were carried out at an open circuit potential. The titanium with an exposed surface area of 1 cm^2 was used as the working electrode. The impedance spectra were acquired in the frequency range of 10^5-10^{-2} Hz with a voltage perturbation amplitude of 10 mV. The EFM method was used with a multiplexer frequency of 2 and 5 Hz with 4 cycles. The amplitude of the excitation signal was 10 mV.

Table 1 shows the experimental setup and the sample labels used in this work. There were samples with and without thermal or sandblasting treatment. A raw titanium plate sample was included for comparison purposes. The labels of the nanotube samples were given according to

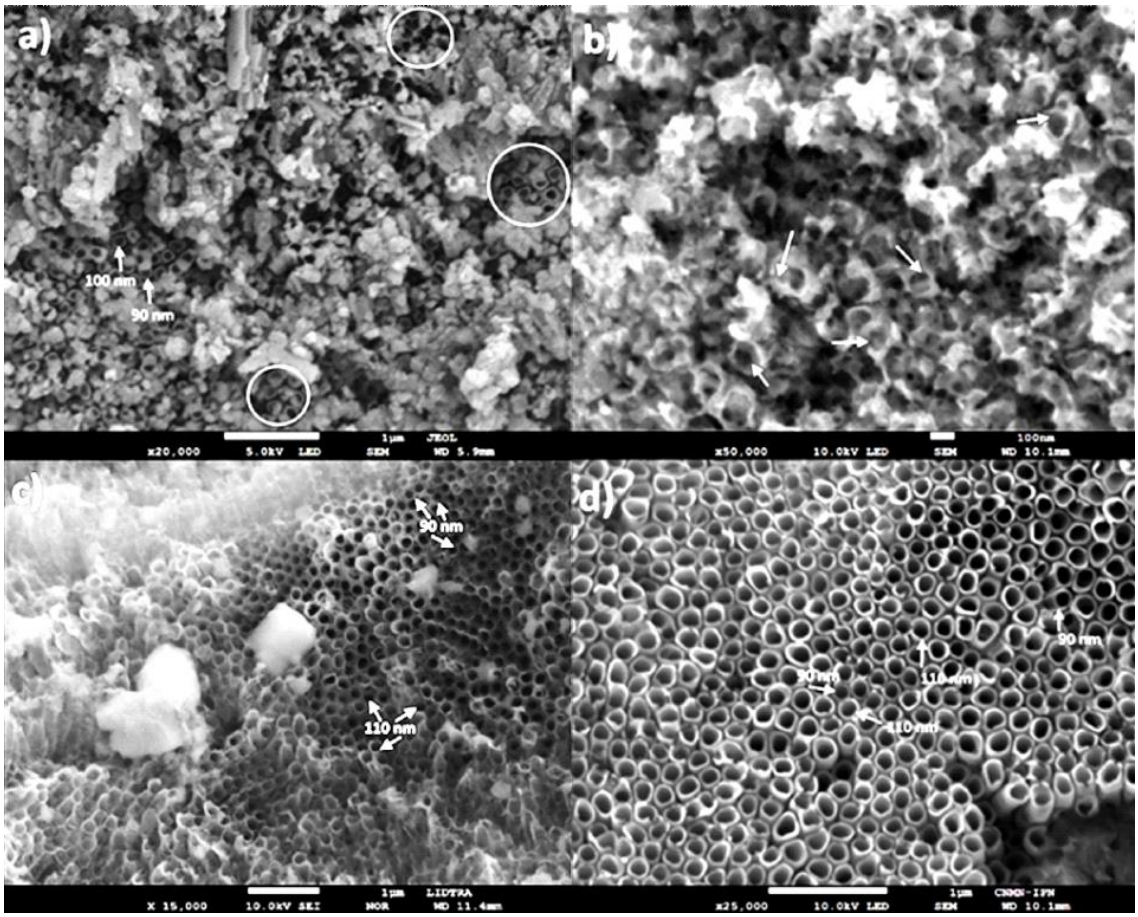

Fig. 1 SEM image of the samples a) NT; b) NT-480; c) NTSB; d) NTSB-480. The range of inner diameters is marked (90-110 nm)

their treatment, modifying either the surface or applying heat treatment or both. NT corresponds to anodized Ti, which generated nanotubes (NT). NT-480 corresponds to anodized heat treated Ti at about 480°C for 1 h to obtain the anatase phase (Chang *et al*. 2011). NTSB corresponds to Ti plates, whose surface was first mechanically modified using sandblast, and then after, anodized to obtain a structure with nanotubes. NTSB-480 corresponds to Ti plates, whose surface were first mechanically modified using sandblast, anodized, and heat-treated to 480°C for 1 h.

3. Results and discussion

3.1 Anodization of Ti morphology and composition

Fig. 1(a) shows the SEM image of the NT array as-anodized. The sample was covered with debris (Yoriya *et al*. 2007). The proposed mechanism for explaining these fragments is that long nanotubes increment the probability of breakage. The chemical composition of the nanotube structure includes fluoride in the form of NH_4TiOF_3 (Zamudio Torres *et al*. 2016a, b). In this figure, some areas are circled; these show the nanotubes with an inner diameter between 90 to 100 nm.

Fig. 1(b) shows the SEM image corresponding to the sample labeled as NT-480. In the figure, fractures in the top of the tube are indicated by arrows; therefore, the tubular structures are difficult to observe due to destruction and coalescence at the top of nanotube walls.

Fig. 1(c) shows the SEM image of the sample NTSB, which shows that the nanotubes grew up in different orientations due to the irregularity in the surface caused by the sandblasting. This result indicates that the nanotube structure grew perpendicular to the surface, in spite of its angle. Thus, the heterogeneous orientation of nanotubes is characteristic of the sandblasted surfaces. The inner diameters of nanotubes are marked in the figure, between 90 to 110 nm, and the length of the tubes reached up to 5 μm (S1).

Fig. 1(d) shows the SEM image corresponding to the sample NTSB-480. It is observed that there are no perceptible physical changes to the NTSB sample. The inner diameters of nanotubes are marked in the figure, which are in the range from 90 to 110 nm. A noticeable difference among the samples NTSB and NTSB-480, differing in the thermal treatment, is the change in chemical composition and crystalline structure, which changed NH_4TiOF_3 to TiO_2 anatase (Zamudio Torres *et al*. 2016a, b).

Figs. 1(a)-(b) differ from Figs. 1(c)-(d) mainly in the sandblasting pre-treatment, which caused coarse surfaces. The effect was a remarkable diminishment in the breakage of the nanotubular structure.

The chemical compositions were analyzed for different

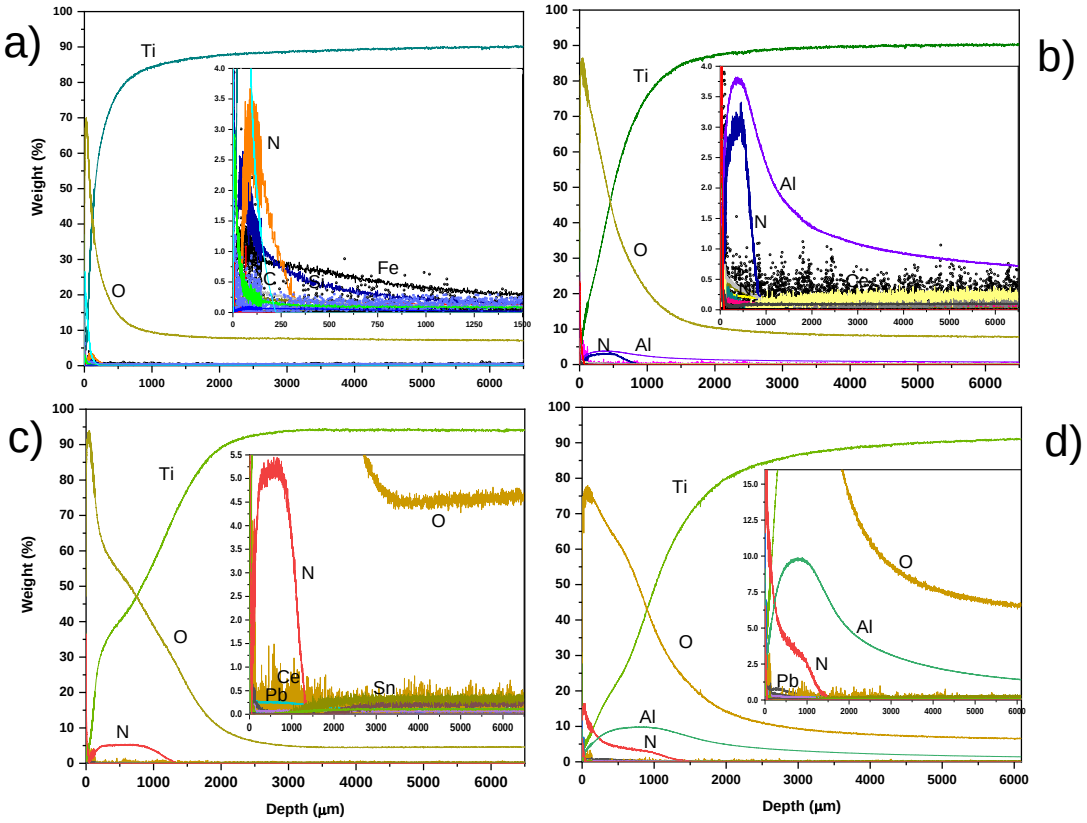

Fig. 2 Chemical depth profiles obtained using GDOES: (a) Substrate with a sandblasting mechanical treatment; (b) and (c) correspond to the samples of TiO_2 nanotubes using a substrate without and with sandblasting (Al_2O_3 grits about 4 mm in size), respectively; (d) profile of a sample having the transformation of TiO_2 nanotubes to TiO_2 anatase nanoparticles

samples using the Glow Discharge Optical Emission Spectroscopy (GDOES). The values of Ti varies in the range of 90-95 wt. % and the oxygen in the range 3.8-8.0 wt. %. A typical substrate composition analyzed by GDOES was approximately Ti 94.11%, O 4.55%, Sn 0.35%, Co 0.23%, Pb 0.12%, V 0.12%, S 0.11%, Mg 0.062%, Fe 0.047%, Mn 0.043%, Mo 0.02%, Cr 0.015%, Ni 0.0055%, and other elements. This composition was relative among the analyzed elements. Fluor was not included in the spectrometer analysis but was identified in previous studies (Zamudio Torres *et al.* 2016a, b), which form the ammonium oxofluorotitanate NH_4TiOF_3 compound.

Fig. 2(a) represents a substrate with a sandblasting mechanical treatment. The titanium substrates were partially oxidized. The inset shows a close-up of the minority elements, such as Sn, Co, Pb, V, S, Mg, Fe, Mn, Mo, Cr, and Ni. Figs. 2(b) and (c) correspond to the samples of TiO_2 nanotubes using a substrate without and with sandblasting (Al_2O_3 grits about 4 mm in size). The presence of Al in the sandblasted surfaces was because of incrusted residues of alumina by the mechanical treatment. Nitrogen reveals the presence of the Ammonium oxofluorotitanate NH_4TiOF_3. The content was in the range 3-15 wt. % and about 1 μm in depth. This implies that the rest of the nanotubes was composed of TiO_2, including the passive layer between the nanotube bottom and the substrate, which was tested with four electrochemical techniques.

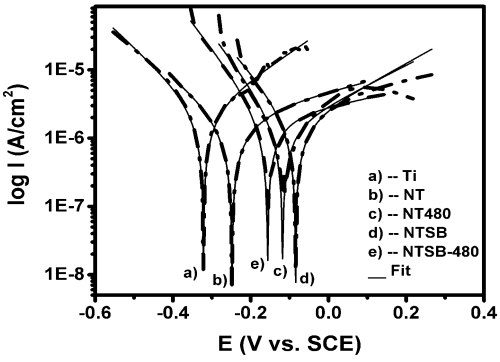

Fig. 3 Measured (- -) and fitted (—) Tafel polarization curves for (a) Ti; (b) NT; (c) NT-480; (d) NTSB; (e) NTSB-480 in 5% NaCl solution

Fig. 2(d) represents the sample having the transformation of NH_4TiOF_3/TiO_2 nanotubes to TiO_2 anatase nanoparticles.

3.2 Analysis of Tafel slops

Fig. 3 shows the Tafel polarization curves for the samples a) Ti, b) NT, c) NT-480, d) NTSB and e) NTSB-480. The experimental data and its fit are shown with dash line and continuous line, respectively. For all samples, there was no breakdown of the passive layers occurring in the

Table 2 Electrochemical parameters obtained from anodic and cathodic Tafel polarization curves of Ti, NT, NT-480, NTSB and NTSB-480 in 5% NaCl solution

Sample	$-E_{corr}$ (mV)	i_{corr} (μA/cm^2)	β_a (mV/dec)	β_C (mV/dec)	CR (mpy)
Ti-alloy	322	2.45	258.2	189	1.119
NT	248	2.18	714.6	251.6	0.9966
NT-480	118	1.36	341.1	130.9	0.5013
NTSB	84.5	1.56	315.6	150.2	0.7144
NTSB-480	156	1.88	818.9	136.3	0.6901

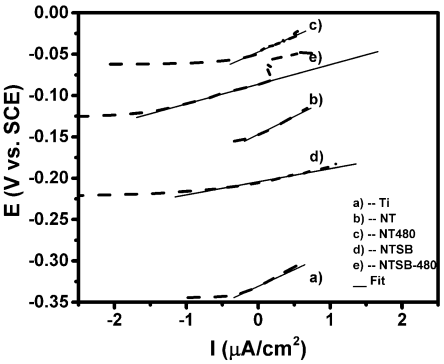

Fig. 4 Potential-Current curves using LPR technique for (a) NT; (b) NT-480; (c) NTSB; (d) NTSB-480 in 5% NaCl solution

Table 3 Results of the potential-current curves

Sample	$-E_{corr}$ (mV)	i_{corr} (μA/cm^2)	β_a (mV/dec)	β_C (mV/dec)	R_p (k Ω cm^2)	CR (mpy)
Ti-alloy	330.8	1.174	258.2	189	40.3	0.53
NT	147.5	1.101	714.6	251.6	43.02	0.50
NT-480	49.68	1.08	341.1	130.9	38.02	0.49
NTSB	205.4	2.792	315.6	150.2	15.8	0.27
NTSB-480	86.85	2.174	818.9	136.3	23.3	0.79

range of the tested potential. This indicates that the layers of NH_4TiOF_3 and TiO_2 nanotubes formed on the surface of Ti and Ti-SB were homogeneous and protective (Bolat *et al*. 2015).

Electrochemical parameters derived from Tafel extrapolation (Bolat *et al*. 2015), cathodic (β_c) and anodic (β_a), corrosion potential (E_{corr}), corrosion current density (i_{corr}), and corrosion rate (CR) were obtained and listed in Table 2.

The data show that Ti have the highest value in CR, followed by the samples of NH_4TiOF_3 (NT and NTSB), and the samples of anatase TiO_2 (NT-480 and NTSB-480) with the lower CR values. The formation of an oxide layer on titanium has an influence on the corrosion protection, which causes a difference between the titanium and the other samples. Nevertheless, neither in the sandblast mechanical treatment nor in the heat treatment, there was a tendency. The NT-480 samples show the lower CR value, which is related to the heat treatment and the anatase TiO_2 layer.

The sandblast mechanical surface treatment changed the roughness. The titanium had a *Ra* (average roughness) of about 0.38 μm, in the case of NT was about 5.74 μm, about 3.5 μm for NT-480, 5.53 for NTSB and 4.55 μm for NTSB-480. The samples with nanotubes on their surface show roughness values similar to those obtained by the sandblasting treatment.

3.3 Analysis of Tafel slops

Fig. 4 shows the potentiodynamic polarization curves for the samples above mentioned, as well as its fitting curves calculated by the Echem Analyst 6.25 software. The continuous lines on the graph correspond to experimental data of the sample using LPR technique. The linear fits of experimental data are shown as dashed lines. From the experimental fitted lines, the corrosion rates and polarization resistances were calculated.

The calculation of corrosion rate using LPR technique is based on few fundamental assumptions, such as that the corrosion rate is uniform, both anodic and cathodic reactions are under activation control (kinetic control), an almost negligible solution resistance, and most importantly, known values of Tafel slopes. Parameters obtained previously from analysis of the cathodic (β_c) and anodic (β_a) Tafel slopes were used to calculate the values corresponding to polarization resistance (R_p), corrosion potential (E_{corr}), current density (i_{corr}), and corrosion rate (CR) using Gamry software. These data are listed in Table 3.

From Table 3, using LPR, it can be noticed that the trend of the results for the corrosion rate is similar to the results previously shown, specifically for the first three samples. However, the higher I_{corr} and lower R_p values for the samples with sandblast pre-treatment were atypical. This means that these samples were less resistant to the corrosion, and this result is opposite to the previous result. This can be attributed to a breakage of the passive layer and, in this case, due to the sandblast pre-treatment, a higher amount of area for the Ti-alloy substrate (see Fig. 4(e)).

3.4 Electrochemical impedance spectroscopy (EIS)

Fig. 5 shows the Nyquist plot for a) Ti sample, b) NT, c) NT-480, d) NTSB and e) NTSB-480. In the plots, the squares are the experimental data and the red solid lines are the fit for the CPE with a diffusion model (Jayaraman *et al*. 2010, Saha *et al*. 2010, Paul *et al*. 2014). The equivalent circuit for the CPE with a diffusion model is shown in Fig. 5(f). For the circuit model, R_p is the polarization resistance, W_d the Warburg diffusion, R_u is the solution resistance, Y_0 is the value of the constant phase element, and α is the CPE Y_0 value of the preventive layer capacitance.

Nyquist plots recorded for the different samples above mentioned in 5% NaCl solution do not produce perfect semicircles as expected from the theory of EIS. This deviation of the ideal semicircle is attributed to the frequency dispersion, heterogeneity at the surface, and porosity. The presence of a constant Warburg (W_d) impedance in the circuit confirms that the mass transport is limited by the surface passive layer (Al-Mobarak *et al*.

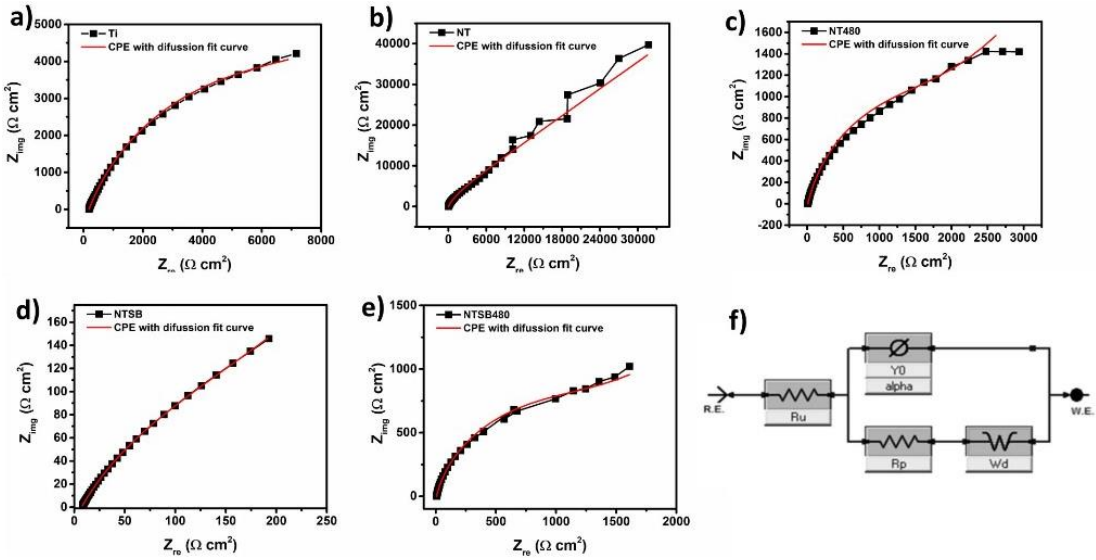

Fig. 5 Nyquist plots of measured (■) and simulated (—) complex plane impedance of (a) Ti; (b) NT; (c) NT-480; (d) NTSB; (e) NTSB-480 in 5% NaCl solution; (f) equivalent circuit used to model impedance data for Ti and different samples of anodized Ti. The tests were done in 5% NaCl solutions

Table 4 Electrochemical parameters obtained from EIS technique after the fitted Nyquist plot and the corresponding equivalent circuit

Sample	R_u (Ω)	Y_0 (S × s$^{\alpha}$)	α	W_d (S × s$^{1/2}$)	R_{ct} (kΩ)	β_a (mV/dec)	β_C (mV/dec)	i_{corr} (μA/cm^2)	CR (mpy)	Goodness of fit
Ti	183.4	7.985 E^{-5}	0.71	0.4602 E^{-3}	9.5	258.2	189	4.9	3.4	2.024 E^{-4}
NT	8.5	6.649 E^{-5}	0.83	66.42 E^{-6}	57.5	714.6	251.6	1.4	1.0	0.01321
NT-480	8.1	6.626 E^{-4}	0.79	0.00216	22.1	341.1	130.9	1.8	0.68	0.0125
NTSB	7.2	125.4 E^{-6}	0.64	521.5 E^{-6}	48.3	315.6	150.2	0.91	0.65	1.24 E^{-4}
NTSB-480	8.8	0.0015	0.84	0.00421	26.8	818.9	136.3	1.9	0.69	0.003233

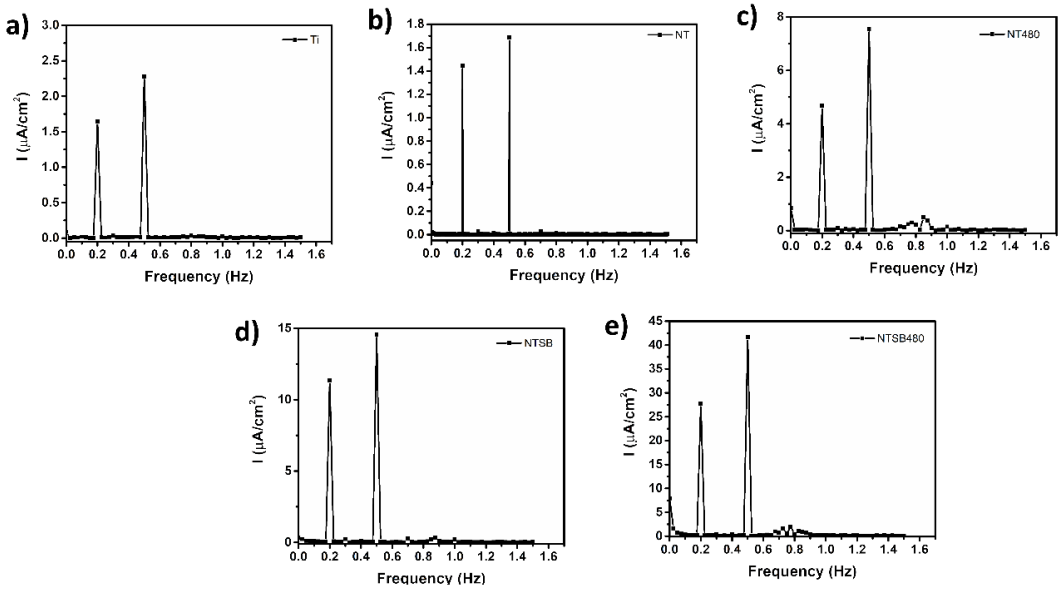

Fig. 6 Intermodulation spectra for (a) Ti plate; (b) NT; (c) NT-480; (d) NTSB; (e) NTSB-480 in 5% NaCl solution

2011, Patil *et al*. 2011, Dhibar *et al*. 2013).

Table 4 shows that the NTSB sample has the same behavior as presented in the technique previously used and the trends in CR are similar.

3.5 Electrochemical frequency modulation (EFM)

Figs. 6(a)-(e) show the frequency spectrum of the current response, in 5% NaCl solution, of a) Ti plate, b) NT,

Table 5 Electrochemical parameters obtained from EFM technique

Sample	i_{corr} (μA/cm^2)	β_a (mV/dec)	β_C (mV/dec)	Causality factor (2)	Causality factor (3)	*CR* (mpy)
Ti-alloy	3.409	108.7	118	1.216	2.647	2.33
NT	1.101	117.7	130.2	1.649	2.277	1.439
NT-480	1.103	112.5	141.8	2.869	3.456	0.4051
NTSB	0.4772	159.3	232.1	1.515	2.738	0.3394
NTSB-480	0.6244	110.4	125	1.931	2.779	0.2294

c) NT-480, d) NTSB and e) NTSB-480. The harmonic and intermediation peaks are observed in the plots. They are clearly visible and higher than the background noise. In all the cases, there are two intense peaks. It is important to note that between the peaks, there is nearly no current response. The experimental EFM data were treated using the activation model. It means, a set of three non-linear equations had been solved, assuming that the corrosion potential does not change due to the polarization of the working electrode (Rauf and Bogaerts 2009, 2010, Fouda and Wahed 2011).

Table 5 shows the corrosion kinetic parameters such as inhibition efficiency (EEFM %), corrosion current density (μA/cm^2), Tafel constants (β_a, β_c), and causality factors (CF-2, CF-3). The composition with TiO_2 decreases the corrosion current density (i_{corr}), indicating that a TiO_2 layer inhibits the corrosion of Ti plates. The advantages provided by the EFM technique is the causality factor, which serves as an internal check on the validity of the EFM measurement. The values of causality factors obtained in this work for the different samples are near to the theoretical values of 2 and 3 (Bosch *et al*. 2001).

3.6 Comparison of corrosion rates

The results of the four different electrochemical techniques are summarized in Fig. 7. The differences in the results of the techniques are not looking for a direct comparison between them. These results show a trend in the plot; it is similar for all values in the samples, except for the Ti sample. Nonetheless, it is considered the corrosion rate values did not show a significant difference among the electrochemical techniques used for the tests, considering that all had the same magnitude order for each surface. The general balance is that the trend is similar in all the cases, and therefore the TiO_2 nanotubes layer is less susceptible to have corrosion.

Therefore, the data obtained from Tafel extrapolation, LPR and EIS are in good agreement with the results obtained from EFM.

4. Conclusions

Four electrochemical techniques were used to evaluate the corrosion rate of titanium without and with a nanostructured titanium oxide layer. The variables for these

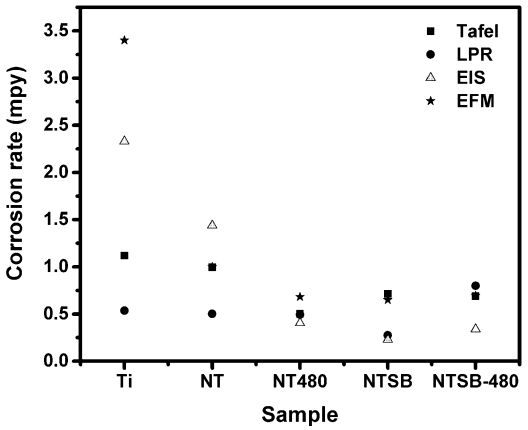

Fig. 7 Summary of the results in corrosion rate obtained by Tafel (■), LPR (●), EIS (▲) and EFM (*) techniques for the samples Ti, NT, NT-480, NTSB and NTSB-480

layers were thermal treatment (480°C) and without and with a sandblasting treatment that increases the area and intended for enhancing the mechanical properties of TiO_2 nanotubes layer, avoiding detachment. The SEM images show a breakage if the nanotube layer for the cases without sandblasting.

The chemical depth profiles show that Ammonium oxofluorotitanate NH_4TiOF_3 was on top of the nanotubes having about 1 μm in depth. This implies that the rest of the nanotubes was composed of TiO_2, including the passive layer between the nanotube bottom and the substrate, whose corrosion behavior was tested.

The corrosion rate values for the tested materials by the four electrochemical techniques show an analogous tendency independently of the technique. In the case of the titanium plate, the values were more disperse from 0.53 mpy to 3.4 mpy.

Using four corrosion measurement techniques was possible to confirm that the TiO_2 nanotubes layer is less susceptible to have corrosion. It was also verified that EFM is a non-destructive corrosion measurement technique that can directly give values of the corrosion current without prior knowledge of Tafel constants. Applying input frequencies used in the EFM technique (2 Hz and 5 Hz), it is possible to obtain results in less than 2 min. An advantage of the EFM technique compared with LPR, EIS and Tafel techniques, is that it validates the data obtained through the causal factors derived from the ratio of amplitudes of harmonic and intermodulation frequencies. In this work, those were close to the theoretical values of 2 and 3 factors.

Acknowledgments

The research described in this paper was financially supported by the National Council of Science and Technology (CONACYT, Grants CEMIE-Sol No. 207450 and LNMG 299124). Thanks to the Center of Nanoscience and Micro and Nanotechnologies for its help in obtaining SEM results, especially to Hugo Martínez Gutiérrez and Héctor Mendoza De León.

References

Al-Mobarak, N.A., Khaled, K.F., Hamed, M.N.H. and Abdel-Azim, K.M. (2011), "Employing electrochemical frequency modulation for studying corrosion and corrosion inhibition of copper in sodium chloride solutions", *Arab. J. Chem.*, **4**, 185-193. https://doi.org/10.1016/j.arabjc.2010.06.036.

Bolat, G., Izquierdo, J., Gloriant, T., Chelariu, R., Mareci, D. and Souto, R.M. (2015), "Investigation of processing effects on the corrosion resistance of Ti20Mo alloy in saline solutions", *Corros. Sci.*, **98**, 170-179. https://doi.org/10.1016/j.corsci.2015.05.025.

Bosch, R.W. and Bogaerts, W.F. (1996), "Instantaneous corrosion rate measurement with small-amplitude potential inter-modulation techniques", *Corrosion*, **52**, 204-212. https://doi.org/10.5006/1.3292115.

Bosch, R.W., Hubrecht, J., Bogaerts, W.F. and Syrett, B.C. (2001), "Electrochemical frequency modulation: A new electrochemical technique for online corrosion monitoring", *Corrosion*, **57**, 60-70. https://doi.org/10.5006/1.3290331.

Chang, Y.J., Lee, J.W., Chen, H.P., Liu, L.S. and Weng, G.J. (2011), "Photocatalytic characteristics of TiO_2 nanotubes with different microstructures prepared under different pulse anodizations", *Thin Solid Films*, **519**, 3334-3339. https://doi.org/10.1016/j.tsf.2010.12.155.

Chen, J., Dai, S., Liu, L., Maitz, M.F., Liao, Y., Cui, J., Zhao, A., Yang, P., Huang, N. and Wang, Y. (2021), "Photo-functionalized TiO_2 nanotubes decorated with multifunctional Ag nanoparticles for enhanced vascular biocompatibility", *Bioact. Mater.*, **6**, 45-54. https://doi.org/10.1016/j.bioactmat.2020.07.009.

Dhibar, S., Sahoo, S., Das, C.K. and Singh, R. (2013), "Investigations on copper chloride doped polyaniline composites as efficient electrode materials for supercapacitor applications", *J. Mater. Sci. Mater. Electron.*, **24**, 576-585. https://doi.org/10.1007/s10854-012-0800-z.

Fouda, A.S. and Wahed, H.A.A. (2011), "Corrosion inhibition of copper in HNO_3 solution using thiophene and its derivatives", *Arab. J. Chem.*, **9**, 591-599. https://doi.org/10.1016/j.arabjc.2011.02.014.

Fraoucene, H., Hatem, D., Vacandio, F. and Pasquinelli, M. (2019), "TiO_2 nanotubes with nanograss structure: The effect of the anodizing voltage on the formation mechanism and structure properties", *J. Electron. Mater.*, **48**, 2046-2054. https://doi.org/10.1007/s11664-019-06951-y.

Ge, M., Li, Q., Cao, C., Huang, J., Li, S., Zhang, S., Chen, Z., Zhang, K., Al-Deyab, S.S. and Lai, Y. (2017), "One-dimensional TiO_2 Nanotube Photocatalysts for Solar Water Splitting", *Adv. Sci.*, **4**, 1600152. https://doi.org/10.1002/advs.201600152.

Genova-Koleva, R.V., Alcaide, F., Álvarez, G., Cabot, P.L., Grande, H.J., Martínez-Huerta, M.V. and Miguel, O. (2019), "Supporting IrO_2 and $IrRuO_x$ nanoparticles on TiO_2 and Nb-doped TiO_2 nanotubes as electrocatalysts for the oxygen evolution reaction", *J. Energy Chem.*, **34**, 227-239. https://doi.org/10.1016/j.jechem.2019.03.008.

Gu, S., Marianov, A.N., Zhu, Y. and Jiang, Y. (2021), "Cobalt porphyrin immobilized on the TiO_2 nanotube electrode for CO_2 electroreduction in aqueous solution", *J. Energy Chem.*, **55**, 219-227. https://doi.org/10.1016/j.jechem.2020.06.067.

Jayaraman, S., Rajarathnam, D. and Srinivasan, M.P. (2010), "Formation of polythiophene multilayers on solid surfaces by covalent molecular assembly", *Mater. Sci. Eng. B*, **168**, 45-54. https://doi.org/10.1016/j.mseb.2010.01.052.

Jovanović, T., Milikić, J., Cvjetićanin, N., Stojadinović, S. and Šljukić, B. (2020), "Performance of Au/Ti and Au/TiO_2 nanotube array electrodes for borohydride oxidation and oxygen reduction reaction in alkaline media", *Electroanalysis*, **32**, 1867-1874. https://doi.org/10.1002/elan.202060015.

Kuş, E. and Mansfeld, F. (2006), "An evaluation of the electrochemical frequency modulation (EFM) technique", *Corros. Sci.*, **48**, 965-979. https://doi.org/10.1016/j.corsci.2005.02.023.

Li, B., Anwer, S., Huang, X., Luo, S., Fu, J. and Liao, K. (2021), "Nitrogen-doped carbon encapsulated in mesoporous TiO_2 nanotubes for fast capacitive sodium storage", *J. Energy Chem.*, **55**, 202-210. https://doi.org/10.1016/j.jechem.2020.06.074.

Liu, Y., Wan, L., Wang, J., Cheng, L., Chen, R. and Ni, H. (2020), "Binary electrocatalyst composed of Mo_2C nanocrystals with ultra-low Pt loadings anchored in TiO_2 nanotube arrays for hydrogen evolution reaction", *Appl. Surf. Sci.*, **509**, 144679. https://doi.org/10.1016/j.apsusc.2019.144679.

Mazare, A., Totea, G., Burnei, C., Schmuki, P., Demetrescu, I. and Ionita, D. (2016), "Corrosion, antibacterial activity and haemocompatibility of TiO_2 nanotubes as a function of their annealing temperature", *Corros. Sci.*, **103**, 215-222. https://doi.org/10.1016/j.corsci.2015.11.021.

McIntyre, P.J. and Mercer, A.D. (2010), "2.34 - corrosion testing and determination of corrosion rates, in: Shreir's corrosion", 1443-1526. http://dx.doi.org/10.1016/B978-044452787-5.00073-1.

Noh, K.J., Nam, I. and Han, J.W. (2020), "Nb-TiO_2 nanotubes as catalyst supports with high activity and durability for oxygen reduction", *Appl. Surf. Sci.*, **521**, 146330. https://doi.org/10.1016/j.apsusc.2020.146330.

Ouyang, W., Teng, F. and Fang, X. (2018), "High performance BiOCl nanosheets/TiO_2 nanotube arrays heterojunction UV photodetector: the influences of self-Induced inner electric fields in the BiOCl nanosheets", *Adv. Funct. Mater.*, **28**, 1707178. https://doi.org/10.1002/adfm.201707178.

Patil, D.S., Shaikh, J.S., Dalavi, D.S., Karanjkar, M.M., Devan, R.S., Ma, Y.R. and Patil, P.S. (2011), "An Mn doped polyaniline electrode for electrochemical supercapacitor", *J. Electrochem. Soc.*, **158**, 653-657. https://doi.org/10.1149/1.3561428.

Paul, S., Pattanayak, A. and Guchhait, S.K. (2014), "Corrosion behavior of carbon steel in synthetically produced oil field seawater", *Int. J. Met.*, **2014**, 1-11. https://doi.org/10.1155/2014/628505.

Rauf, A. and Bogaerts, W.F. (2009), "Monitoring of crevice corrosion with the electrochemical frequency modulation technique", *Electrochim. Acta*, **54**, 7357-7363. https://doi.org/10.1016/j.electacta.2009.07.066.

Rauf, A. and Bogaerts, W.F. (2010), "Employing electrochemical frequency modulation for pitting corrosion", *Corros. Sci.*, **52**, 2773-2785. https://doi.org/10.1016/j.corsci.2010.04.016.

Saha, J.K., Mitra, P.K., Paul, S. and Singh, D.D.N. (2010), "Performance of different organic coatings on steel substrate by accelerated and in atmospheric exposure tests", *Indian J. Chem. Technol.*, **17**, 102-110.

Santamaria, M., Conigliaro, G., Di Franco, F., Megna, B. and Di Quarto, F. (2017), "Electronic properties of thermal oxides on Ti and their influence on impedance and photoelectrochemical behavior of TiO_2 nanotubes", *J. Electrochem. Soc.*, **164**, 113-120. https://doi.org/10.1149/2.0601704jes.

Schlicht, S., Büttner, P. and Bachmann, J. (2019), "Highly active Ir/TiO_2 electrodes for the oxygen evolution reaction using atomic layer deposition on ordered porous substrates", *ACS Appl. Energy Mater.*, **2**, 2344-2349. https://doi.org/10.1021/acsaem.9b00402.

Shang, F., Chen, S., Liang, J. and Liu, C. (2018), "The photocatalytic properties and mechanistic study of ZnO, Ag multiphase Co-composited TiO_2 nanotube arrays film prepared by one-step anodization method", *J. Electrochem. Soc.*, **165**, 258-265. https://doi.org/10.1149/2.0251807jes.

Sierra-Uribe, H., Córdoba-Tuta, E.M. and Acevedo-Peña, P.

(2017), "The effect of the heating rate on anatase crystal orientation and its impact on the photoelectrocatalytic performance of TiO_2 nanotube arrays", *J. Electrochem. Soc.*, **164**, 279-285. https://doi.org/10.1149/2.0241706jes.

Sumi, H., Shimada, H., Yamaguchi, Y. and Yamaguchi, T. (2017), "Effect of anode thickness on polarization resistance for metal-supported microtubular solid oxide fuel cells", *J. Electrochem. Soc.*, **164**, 243-247. https://doi.org/10.1149/2.0431704jes.

Supraja, N., Avinash, B. and Prasad, T.N.V.K.V. (2017), "*Nelumbo nucifera* extracts mediated synthesis of silver nanoparticles for the potential applications in medicine and environmental remediation", *Adv. Nano Res., Int. J.*, **5**(4), 373-392. https://doi.org/10.12989/anr.2017.5.4.373.

Tho, N.T., Thi, C.M., Van Hieu, L. and Van Viet, P. (2020), "Visible-light-driven photocatalysis for methylene blue degradation and hydrogen evolution reaction: A case of black TiO_2 nanotube arrays", *J. Aust. Ceram. Soc.*, **56**, 849-857. https://doi.org/10.1007/s41779-019-00405-8.

Wang, S., Guan, B.Y., Yu, L. and Lou, X.W.D. (2017), "Rational design of three-layered TiO_2@Carbon@MoS_2 hierarchical nanotubes for enhanced lithium storage", *Adv. Mater.*, **29**, 1702724. https://doi.org/10.1002/adma.201702724

Wang, S., Zhang, Z., Huo, W., Zhang, X., Fang, F., Xie, Z. and Jiang, J. (2021), "Single-crystal-like black Zr-TiO_2 nanotube array film: An efficient photocatalyst for fast reduction of Cr(VI)", *Chem. Eng. J.*, **403**, 126331. https://doi.org/10.1016/j.cej.2020.126331.

Xu, L., Niu, J., Xie, H., Ma, X., Zhu, Y. and Crittenden, J. (2021), "Effective degradation of aqueous carbamazepine on a novel blue-colored TiO_2 nanotube arrays membrane filter anode", *J. Hazard. Mater.*, **402**, 123530. https://doi.org/10.1016/j.jhazmat.2020.123530.

Yoriya, S., Paulose, M., Varghese, O.K., Mor, G.K. and Grimes, C.A. (2007), "Fabrication of vertically oriented TiO_2 nanotube arrays using dimethyl sulfoxide electrolytes", *J. Phys. Chem. C*, **111**, 13770-13776. https://doi.org/10.1021/jp074655z.

Zamudio Torres, I., Pérez Bueno, J.D.J., Torres López, C.Y., Lartundo Rojas, L., Mendoza López, M.L. and Vong, Y.M. (2016a), "A phenomenon of degradation of methyl orange observed during the reaction of NH_4TiOF_3 nanotubes with the aqueous medium to produce TiO_2 anatase nanoparticles", *RSC Adv.*, **6**, 76167-76173. https://doi.org/10.1039/C6RA15149C.

Zamudio Torres, I., Pérez Bueno, J.D.J., Torres López, C.Y., Lartundo Rojas, L., Mendoza López, M.L. and Vong, Y.M. (2016b), "Nanotubes with anatase nanoparticulate walls obtained from NH_4TiOF_3 nanotubes prepared by anodizing Ti", *RSC Adv.*, **6**, 41637-41643. https://doi.org/10.1039/C6RA05738A.

Zhao, C., Yu, C., Zhang, M., Huang, H., Li, S., Han, X., Liu, Z., Yang, J., Xiao, W., Liang, J., Sun, X. and Qiu, J. (2017), "Ultrafine MoO_2-Carbon microstructures enable ultralong-life power-type sodium ion storage by enhanced pseudo-capacitance", *Adv. Energy Mater.*, **7**, 1602880. https://doi.org/10.1002/aenm.201602880.

Zhou, X., Liu, N. and Schmuki, P. (2017), "Photocatalysis with TiO_2 nanotubes: 'Colorful' reactivity and designing site-specific photocatalytic centers into TiO_2 nanotubes", *ACS Catal.*, **7**, 3210-3235. https://doi.org/10.1021/acscatal.6b03709.